Environmental Pollution 283 (2021) 117104

Contents lists available at ScienceDirect

Environmental Pollution

journal homepage: www.elsevier.com/locate/envpol

The decomposition of macrozoobenthos induces large releases of phosphorus from sediments

Xiaolei Xing [a], Musong Chen [b, *], Yuexia Wu [b], Yazhou Tang [b], Cai Li [b]

[a] College of Hydrology and Water Resources, Hohai University, Nanjing, 210098, China
[b] State Key Laboratory of Lake Science and Environment, Nanjing Institute of Geography and Limnology, Chinese Academy of Sciences, Nanjing, 210008, China

ARTICLE INFO

Article history:
Received 9 October 2020
Received in revised form
24 March 2021
Accepted 5 April 2021
Available online 10 April 2021

Keywords:
Macrozoobenthos decomposition
High resolution technique
Dissolved organic matter
Phosphorus
Sediment-water interface

ABSTRACT

Lake eutrophication and algal blooms may result in the mortality of macrozoobenthos. However, it is still not clear how macrozoobenthos decomposition affect phosphorus (P) mobility in sediments. High-resolution dialysis (HR-Peeper) and the diffusive gradients in thin films (DGT) technique were used in this study to assess the dissolved organic matter (DOM), dissolved/DGT-labile iron (Fe), P, and sulfur (S(−II)) profiles at a millimeter resolution. The decomposition of *Bellamya aeruginosa* significantly increased the internal loading of sediments P. The Fe(III) and sulfate were reduced under anaerobic conditions and promoted P desorption from sediments. This was supported by the significant increase in DGT-labile S(−II) and dissolved/DGT-labile P, Fe(II) and the significant positive correlation between Fe and P on day 8. The simultaneous increase in DOM and soluble reactive phosphorus (SRP) and the significant positive relationship between these factors were observed during the decomposition of *B. aeruginosa*. This suggested that complexation of DOM with metals may promotes the release of P from sediments.

1. Introduction

Phosphorus (P), an indispensable element in organisms, constitutes important cellular compounds such as phospholipids and ATP and participates in biochemical reactions (Sannigrahi et al., 2006). It acts directly on the primary productivity of aquatic ecosystems (Herschy et al., 2018; Zhang et al., 2018a, b). As a result of P accumulation, lakes have been subjected to continuous and repeated algae outbreaks in many regions. Limiting P inputs into lakes is an important control measure of solving eutrophication issues (Paerl et al., 2011), but there is low overall progress for some lakes. Sediments inflicts the maintenance and increase of P concentrations in the lake via pore water diffusion and solid phase dissolution (Tang et al., 2020). Qin et al. (2019) propose that sediments, contained about 70% historical external loading of P, is a non-negligible reason for the little long-term treatment effect in Lake Taihu. The progress of sediments P release can be influenced by several environmental factors (redox, pH, organic matter, etc.) (Kraal et al., 2015) and macrozoobenthos which widely distributed near the sediment-water interface (SWI) promote P cycling in shallow lake (Berezina et al., 2019; Gautreau et al., 2020; S. Zhang et al., 2020).

Several studies have investigated the effects of bioturbation of the macrobenthos (e.g., bioirrigation) on sediments P, studying a variety of benthic macroinvertebrates (Chen et al., 2015, 2016). However, macrobenthos are sensitive to environment conditions. Hypoxia and accumulation of phycotoxins caused by eutrophication can destroy the living environment of benthos and local dead water area led to mortality of them (Gu et al., 2020; Lance et al., 2007; Maar et al., 2010; Stachowitsch et al., 2007). Similarly, decomposition may further exacerbate anaerobic conditions and induce P release from sediments (Nędzarek et al., 2015). We hypothesize that benthos mortality and decomposition may be another key factor of P mobility in eutrophication lake, which increase the P concentration in overlying water and may form a vicious circle among benthos, algae bloom and sediments. However, related studies are scarce.

Decomposition changed the redox conditions and greatly affected P cycling, as the phenomenon reflected in studies on common aquatic organisms (such as algae, jellyfish, fish, and aquatic plants) (Chelsky et al., 2016; Li et al., 2015). In previous studies, there were two main contributions of P level during decomposition progress (Chen et al., 2018). Firstly, decomposition

* Corresponding author.
E-mail address: mschen@niglas.ac.cn (M. Chen).

https://doi.org/10.1016/j.envpol.2021.117104
0269-7491/

increases the consumption of dissolved oxygen and causes P desorption from Fe(III) oxyhydroxides near SWI (Gao et al., 2013; Yao et al., 2016). Secondly, organisms contain large amount of nutrients and their residues return P to water column or sediments via. decomposition (Wang et al., 2016). In addition, prior studies have observed that P concentration of overlying water can be increased with the addition of dissolved organic matter (DOM) (Goyne et al., 2008; Wang et al., 2012). The DOM with abundant groups can promote sediments P release via. occupation of the P adsorption sites on metal oxides (or clay particles) and complexes formation with metal which reduced the available metal (such as Fe) levels (Barber et al., 2014; Du et al., 2019; Hunt et al., 2007). However, the role of DOM during decomposition progress is rarely discussed. Accordingly, studying the dynamic of DOM, Fe and P during benthos decomposition is vital with the overall goal to understand P cycling in eutrophic lakes.

With advances in sediments research, the techniques used to investigate P cycling processes have largely been improved. The passive sampling techniques (high-resolution dialysis (HR-Peeper) and the diffusive gradients in thin films (DGT)) can reflect the *in-situ* conditions of sediments. These techniques reduce the oxidation of the target substance, improve the spatial resolution, and deliver accurate results (Gao et al., 2007; Xu et al., 2012).

In this study, we revealed the impact of benthos decomposition on P mobility in Lake Taihu. The variations of P, Fe, DOM, and S(−II) in different decomposition periods and the relationship between P, Fe, and DOM were simultaneously investigated using HR-Peeper and DGT to assess P exchange. This work clarifies the role of benthos decomposition on nutrients cycling and provide insights into P release mechanisms.

2. Materials and methods

2.1. Sampling site

Lake Taihu, as an important water source in China, is a typical freshwater lake. The Taihu basin is situated in the south of the Yangtze River Delta, with a dense urban network and abundant water resources. Due to its geographical location, Lake Taihu is greatly affected by urbanization (Yuan et al., 2014). As a storage of industrial wastewater and domestic sewage, its ecological environment has been severely damaged, with significant impacts on water supply and the economy (Tiehm et al., 2019). Lake Taihu is a eutrophic lake, and this condition requires urgent measures. This study was carried out in Meiliang Bay (31°26′18″ N, 120°11′12″E), which receives polluted water from the rivers Liangxi, Zhihu Gang, and Wujing Gang.

2.2. Experimental set-up

In September 2019, we collected 16 sediment cores (9 × 50 cm) with 30 cm depth of sediments and 10 cm depth of pristine overlying water from the sampling site with a gravity sampler, and the overlying water at the same location was collected with the use of a polyethylene bucket. The sediment cores were sent back to the laboratory quickly and safely, avoiding disturbance to SWI during transportation.

Eighteen sediment cores were selected for the measurement of target nutrients. Six tubes dived to the treatment group (3 sediment cores) and control group (3 sediment cores) were drilled on the sediment-water interface, and a Rhizon sampler (Rhizon CSS, the Netherlands, 2.5 mm in diameter) was horizontally inserted into the sediment core to collect pore water. The remaining sediment cores were divided to control group (3 sediment cores) and treatment group (9 sediment cores) for deployment of HR-Peeper and DGT. First, all sediment cores were incubated in a tank containing about 45 cm depth tap water at 25 °C (the same temperature in sampling site) for 2 days pre-incubation. Subsequently, to each core, except for the tubes of control group, we added eight carcasses of *B. aeruginosa*, followed by incubation for another 36 days. *B. aeruginosa*, which naturally occurs in Taihu Lake, was purchased from the aquatic product market. Moreover, a glass beaker was added same volume of lake water as that in the sediment core and was added 8 carrions for 36 days incubation at 25 °C.

In addition, a sediment core was carefully moved to a rectangular plexiglass container (10 × 10 × 20 cm) with two planar optode (PO) films pre-affixed to the front portion of the inner window for DO and pH measuring. The core was incubated at 25 °C after 15 days of stabilization and *B. aeruginosa* was added later for 36 days incubation. Lake water was filtered and added to the sediment cores every 3−4 days to replenish the loss of water from sampling and evaporation.

2.3. Sampling

The HR-Peeper and DGT probes have been prepared following the described by Xu et al. (2012) and Ding et al. (2010). For the measurement of SRP, dissolved Fe(II), and UV absorbance at 254 nm (UV_{254}), the HR-Peeper probe and Rhizon sampler were applied, while, ZrO-Chelex DGT for labile P/Fe and AgI DGT for labile S(−II) measurements were applied.

We collected 2 mL of pore water from six sediment cores with a Rhizon sampler on 2nd day of pre-incubation prior to the addition of *B. aeruginosa* and every 4 days after the addition of *B. aeruginosa*. Similarly, three sediment cores were selected for HR-Peeper and DGT analysis on 2nd day of pre-incubation prior to the addition of *B. aeruginosa* and on days 8, 16, and 36 after the addition *B. aeruginosa*. The HR-Peeper probe was slowly inserted vertically into each core, and after equilibrium for 24 h, we added ZrO-Chelex DGT and AgI DGT probes for another 24 h. After this period, all probes were retrieved, and the surfaces were carefully cleaned with wet filter paper and deionized water, respectively. And, the sediment cores were measured the speciation of P in the upper 5-cm sediments.

The environment conditions (DO and pH) in sediments were measured using PO technique. The PO method can measure two-dimensional distribution of DO and pH in sediments and water body. The principle of PO was described in studies by Li et al. (2019). After the rectangular sediment cores stabilization and on days 2, 4, 6, 8, 16, 24 and 36 after the addition of *B. aeruginosa*, the DO and pH were measured.

2.4. Chemical and data analyses

The HR-Peeper carried about 400 μL pore water in each chamber, and to obtain the water sample, the cellulose nitrate membrane was pierced for analysis of SRP, dissolved Fe(II) and UV_{254}. After careful cleaning with deionized water, the ZrO-Chelex gels were cut into 2-mm sections. Each section was submerged with 800 μL of 1 M HNO_3, deionized water, and 800 μL of 1 M NaOH in succession. The HNO_3 and NaOH extracts were used for measuring Fe(II) and P, respectively. The AgI gels, scanned with flat-bed scanner, were used for labile S(−II) analysis by computer-imaging densitometry (CID) technique (Ding et al., 2013). Concentrations of Fe(II) and P were determined using the phenanthroline and the molybdenum blue colorimetric methods by Microplate Spectrophotometer (Epoh), respectively (Tamura et al., 1974; Xie et al., 2013). And, the UV_{254} was measured by Microplate Spectrophotometer (Epoh) to analyze the humic acid DOM in the pore water (Krom and Sholkovitz, 1977;

Xu and Guo, 2017; Zhang et al., 2018a, b). The NH_4^+, SO_4^{2-} and Mn^{2+} were measured by Continuous Flow Analyzer (Skalar 5000, the Netherlands), turbidimetric method (Tabatabai, 1974) and Inductively Coupled Plasma Mass Spectrometry (NexION 350X), respectively. The fractionation of P was measured through the developed method by Rydin (Rydin and Welch, 1998).

The images of AgI gels at 600dpi were converted to grayscale density (y), and the accumulated quantity of labile S(−II) per unit area (x) was calculated with Equation (1). Subsequently, C_{DGT} was calculated with Equation (3):

$$y = -171e^{-x/7.23} + 220 \quad (1)$$

The accumulated quantity of Fe or P was calculated using Equation (2):

$$M = C_e V_e / f_e \quad (2)$$

where f_e is the elution efficiency and C_e, V_e is the concentration and volume of the extract, respectively.

The concentrations of labile P, Fe, and S were calculated with Equation (3):

$$C_{DGT} = M\Delta g / DAt \quad (3)$$

where t is the equilibration time; D is the diffusion coefficient of the solute at equilibration temperature; A is the contact area of the gel and sediments; and Δg is the thickness of the diffusive layer (Ding et al., 2010).

All correlation analysis between each two variables were performed using SPSS v20.0 software and all figures were plotted using Origin 8.0 software.

3. Results and discussion

3.1. DO and pH profiles

The pH values of the control group and on days 2, 4, 6, 8, 16, 24, and 36 of the treatment group are shown in Fig. 1. In the control group, the overlying water was weakly alkaline and the pH was slightly greater than that of sediments. The maximum value of pH appeared in the zone above the SWI, and the minimum appeared near the SWI. In deeper sediments, pH value was about 7 with little change in vertical and transverse direction. In the treatment group, the sediments near SWI and overlying water changed dramatically. After the addition of *B. aeruginosa*, the pH slowly decreased and reached to the lowest value in the overlying water column on day 8. The pH of sediments near SWI had the same trend, and the influenced depth of sediments increased with time. After this period, the pH value slowly increased and fluctuated slightly.

The changes in DO, as a result of the decomposition of *B. aeruginosa*, are shown in Fig. 1. The overlying water of sediments

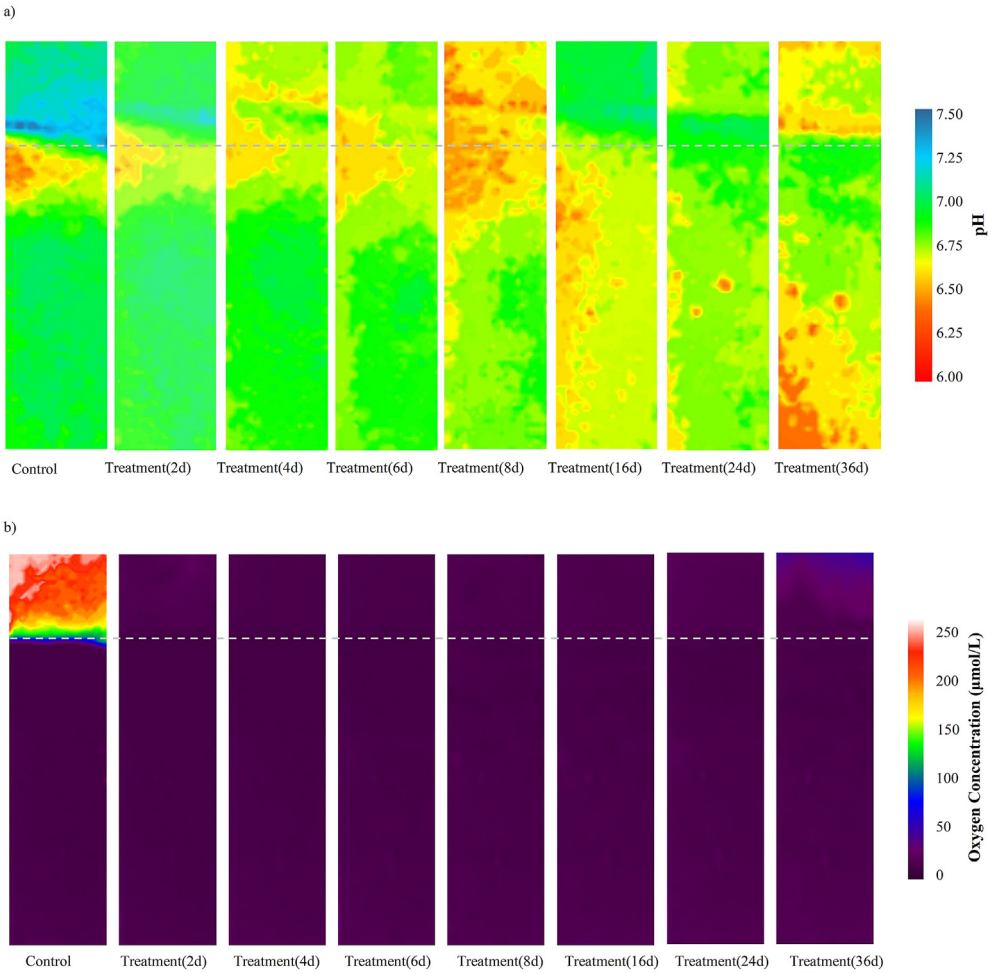

Fig. 1. pH profiles (a) and DO profiles (b) of the sediment samples in the control and in the treatment groups at 2, 4, 6, 8, 16, 24, and 36 days after the addition of *B. aeruginosa*. The dotted line represents the SWI.

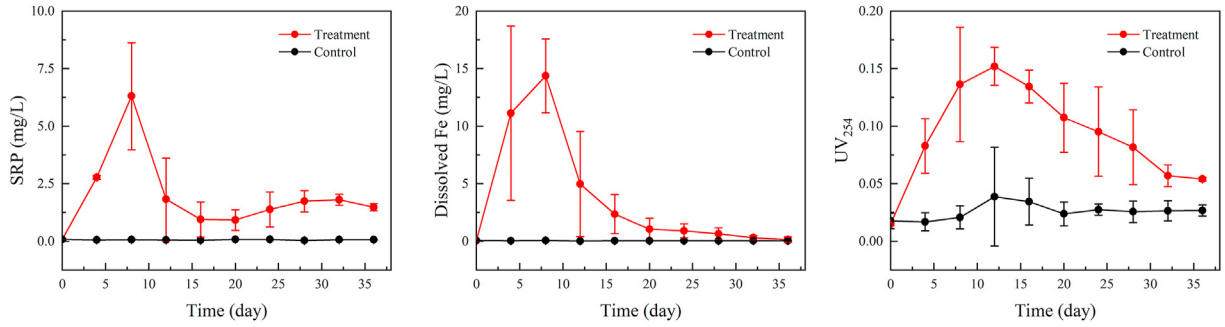

Fig. 2. Changes in the concentrations of SRP (a), dissolved Fe (b), and UV_{254} (c) in the overlying water column of the control group and the treatment group.

in control which exposed to air was rich in dissolved oxygen. The concentration of DO near the water surface was the highest, and then slowly decreased with depth until the SWI. The DO near SWI dropped sharply and remained at a low concentration in sediments. In treatment group, on day 2, the sediments and overlying water were both in anaerobic state with DO concentration close to 0 μmol/L. Subsequently, the whole system remained anaerobic for 2−24 days. Up to 36th day, compare the 6.96 μmol/L on 24th day, the mean DO value of overlying water increased to 20.06 μmol/L. The highest DO concentration occurred at water surface and decreased with depth, while, the sediments and the vicinity of SWI remained anaerobic.

3.2. Changes in overlying water SRP, dissolved Fe, and UV_{254} after *B. aeruginosa* addition

The changes in soluble reactive phosphorus (SRP), dissolved Fe, and UV_{254} in the overlying water column are shown in Fig. 2. Smaller changes were observed in the concentrations of SRP, dissolved Fe, and UV_{254} in control group. While, in treatment group, the concentrations changed dramatically.

The initial concentrations of SRP, dissolved Fe, and UV_{254} in treatment group were 0.088 mg/L, 0.056 mg/L and 0.015 mg/L, respectively. After the addition of *B. aeruginosa*, the levels changed notably. From day 0 to day 8, the SRP and dissolved Fe concentrations increased rapidly and reached maximum values of 6.30 and 14.37 mg/L, respectively. In contrast, the SRP and dissolved Fe concentrations sharply decreased from day 8 to day 12; after this, the SRP concentration fluctuated within a small range, and the dissolved Fe concentration slowly decreased to a stable value. The UV_{254} absorption had a smoother peak, and its concentration significantly increased to the highest value of 0.152 on day 12, followed by a slight and steady decrease until the end of the experiment.

In addition, the SRP consistently changed with changes in the dissolved Fe level. A significant positive correlation between them was observed (Table 1).

3.3. Changes in pore water SRP, dissolved Fe, and UV_{254} with *B. aeruginosa* addition

The changes in the pore water SRP, dissolved Fe concentrations, and UV_{254} absorbance in the sediment profiles with *B. aeruginosa* addition are shown in Fig. 3. The SRP concentrations significantly increased with the decomposition of *B. aeruginosa* from the top to the bottom of the profiles, with the largest increase on day 8, an average of 1779% of the control. After that, the SRP concentration significantly decreased from day 8 to day 36, with a mean SRP reduction by 288.7% on day 36 of that of the control compared with day 8. In all three decomposition periods, the SRP concentration in the overlying water column maintained a high level and decreased slowly in the sediments with depth.

Similarly, the dissolved Fe concentrations significantly increased with the decomposition of *B. aeruginosa* from the top to the bottom. The largest increase of dissolved Fe concentration was found on day 8, with a mean concentration of 876.7% of that of the control. Subsequently, dissolved Fe concentration reached 423.3% on day 36 compared to day 8. Based on the distribution of dissolved Fe, peak levels were obtained near the SWI.

The UV_{254} absorption showed a similar trend; it significantly increased from the deeper to the upper layers throughout all profiles. The largest mean UV_{254} value was observed on day 8 and was 992.3% of that of the control. It rapidly decreased to a value of 482.0% on day 36.

Table 2 shows the Pearson's correlation coefficients between SRP and dissolved Fe/UV_{254}. A significant positive correlation between SRP and dissolved Fe/UV_{254} was observed throughout the experimental period, except for SRP and dissolved Fe on day 36.

3.4. Changes in labile P, labile Fe, and labile S(−II) in sediments with *B. aeruginosa*

The effects of *B. aeruginosa* decomposition on the mobility of labile P/Fe in sediments are shown in Fig. 4. The labile P concentrations significantly increased at the depth from the top to the bottom of the profiles, similar to SRP. The largest mean concentration of labile P was found on day 8 and was 993.0% of that of the control. After this, the labile P concentration decreased to 506.8% of that of the control on day 36. Similarly, the largest mean concentration of labile Fe was found on day 8, with a concentration of 2170% of that of the control. The labile Fe concentration reached 826.7% on day 36. Labile P and Fe were positively correlated ($R^2 \geq 0.596$, $p < 0.01$) in the control group and the day 8 of the treatment group. As decomposition progressed, poor correlations were observed (Table 3).

As shown in Fig. 5, labile S(−II) was also influenced by *B. aeruginosa* decomposition. In the control, labile S(−II) was mainly distributed in the deep anaerobic zone. During the decomposition process, conditions became highly anaerobic, and S(−II) rapidly increased in the overlying water and the upper layer of sediments. The concentration of S(−II) in deeper sediments was almost unchanged. Subsequently, S(−II) slowly decreased in last two periods,

Table 1
Correlation analysis between SRP with Fe and UV_{254} in the overlying water column during *B. aeruginosa* decomposition.

Parameters	R^2	*P* value
SRP vs. dissolved Fe	0.871**	<.01
SRP vs. UV_{254}	0.440	.203

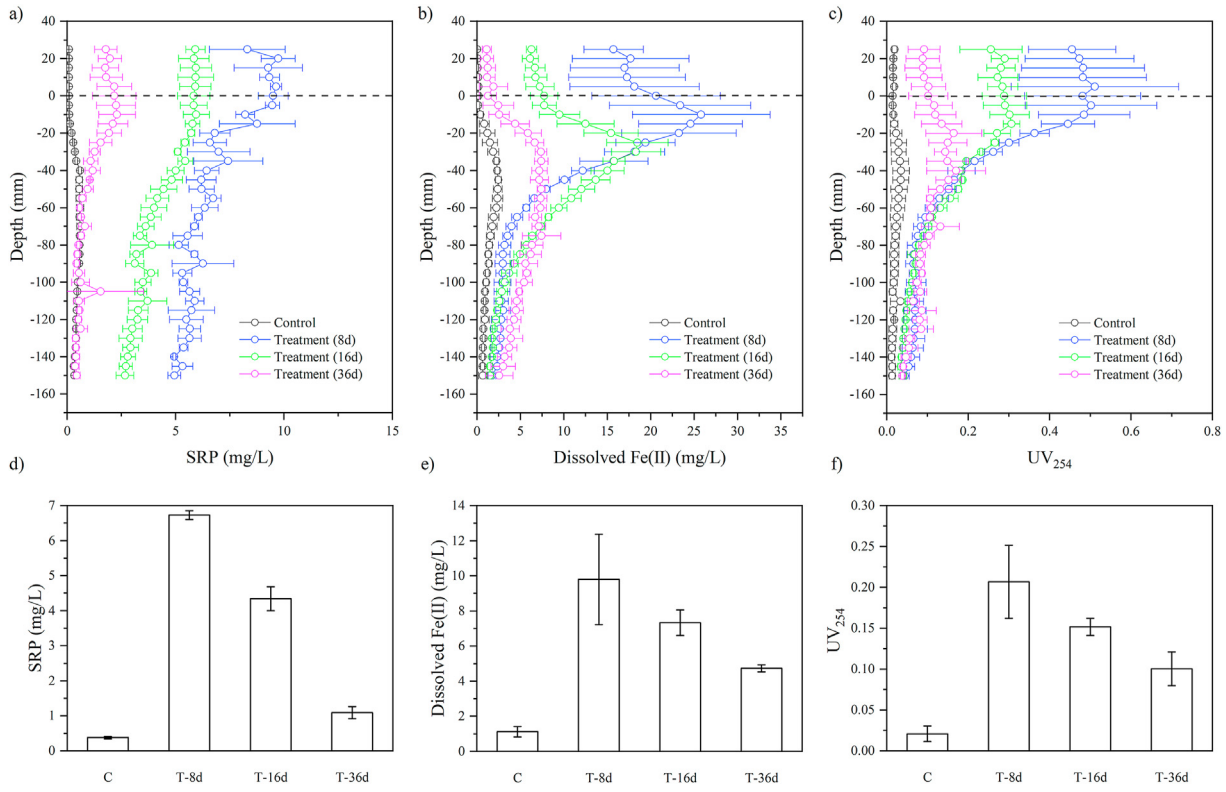

Fig. 3. Distributions of SRP (a), dissolved Fe (b), and UV_{254} (c) in the sediment-water profile and the mean values of SRP (d), dissolved Fe (e), and UV_{254} (f) at the influence depth. C, T-8d/16 d/36 d represents the control group and treatment group on days 8, 16, and 36, respectively.

Table 2
Correlation analyses between SRP and dissolved Fe/UV_{254} in the control and in sediments with the addition of *B. aeruginosa*.

Parameters	Treatments	Time	R^2	*P* value
SRP vs. dissolved Fe	Control		0.791**	<.01
	B. aeruginosa	8 days	0.844**	<.01
		16 days	0.649**	<.01
		36 days	−0.454**	<.01
SRP vs. UV_{254}	Control		0.435**	<.01
	B. aeruginosa	8 days	0.955**	<.01
		16 days	0.976**	<.01
		36 days	0.475**	<.01

which may due to the formation of FeS in sediments (Meng et al., 2019).

3.5. Changes of NH_4^+, Mn^{2+} and SO_4^{2-} in pore water and P speciation in upper 5 cm sediments

The concentration of NH_4^+, Mn^{2+} and SO_4^{2-} in pore water of upper sediments (0–5 cm) were shown in Table S1. After the addition of *B. aeruginosa*, the concentration of NH_4^+ and Mn^{2+} increased significantly. The maximum values were observed on day 8 and then decreased with time. In contrast, the SO_4^{2-} decreased during decomposition and slowly increased on day 36.

The P speciation in upper 5 cm sediments was shown in Fig. S2. Compare to the control group, the concentrations of TP and OP increased in the treatment group and reached the highest value on day 36. The Fe–P and Al–P were slightly decreased on day 8, then increased. While, Ex-P, Ca–P and Res-P were almost unchanged.

3.6. Mechanism of P release from sediments with B. aeruginosa decomposition

According to previous studies, the decomposition of organic residues significantly affects nutrient cycling at the SWI (Wang et al., 2019; Wu et al., 2017). Decomposition is a complex process, and its effect on P mobilization is regulated by multiple mechanisms. The anaerobic conditions, combined with DOM release, induced P release at the SWI (Fig. 6).

B. aeruginosa decomposed quickly in initial days, in the treatment group, the overlying water turned black on day 2 and became noticeably black on day 8. Then, the blackness of water decreased and the water was clear on day 36. In the progress, the decomposition of *B. aeruginosa* dramatically changed the environmental conditions (pH and DO). After the addition of *B. aeruginosa*, a large amount of DOM was released (Fig. 2), resulting in the rapid consumption of oxygen and the generation of acidic substances (CO_2, H_2S and organic acids) (Wang et al., 2015; Zhang et al., 2017; W. Z. Zhang et al., 2020), which caused a decrease in DO and pH (Fig. 1). Subsequently, the concentration of DOM decreased (Fig. 2), resulting in a decrease in the generation of acid gases (CO_2 and H_2S) and the decomposition of organic acids which caused a slow rise in pH (Wang et al., 2016). Simultaneously, the decrease of DOM decreased the DO consumption, and oxygen in the air slowly entered the overlying water, resulting in an increase of DO on the 36th day (Fig. 1b). In addition, the anaerobic state inhibited nitrification and may cause the death of heterotrophic bacteria that released NH_4^+ from lysing cells (Feng et al., 2011), which were the reason for the increase in NH_4^+ (Table S1). And, dead microbial flora decreased the DO consumption which may further contributed to the increase of DO at the end of the experiment.

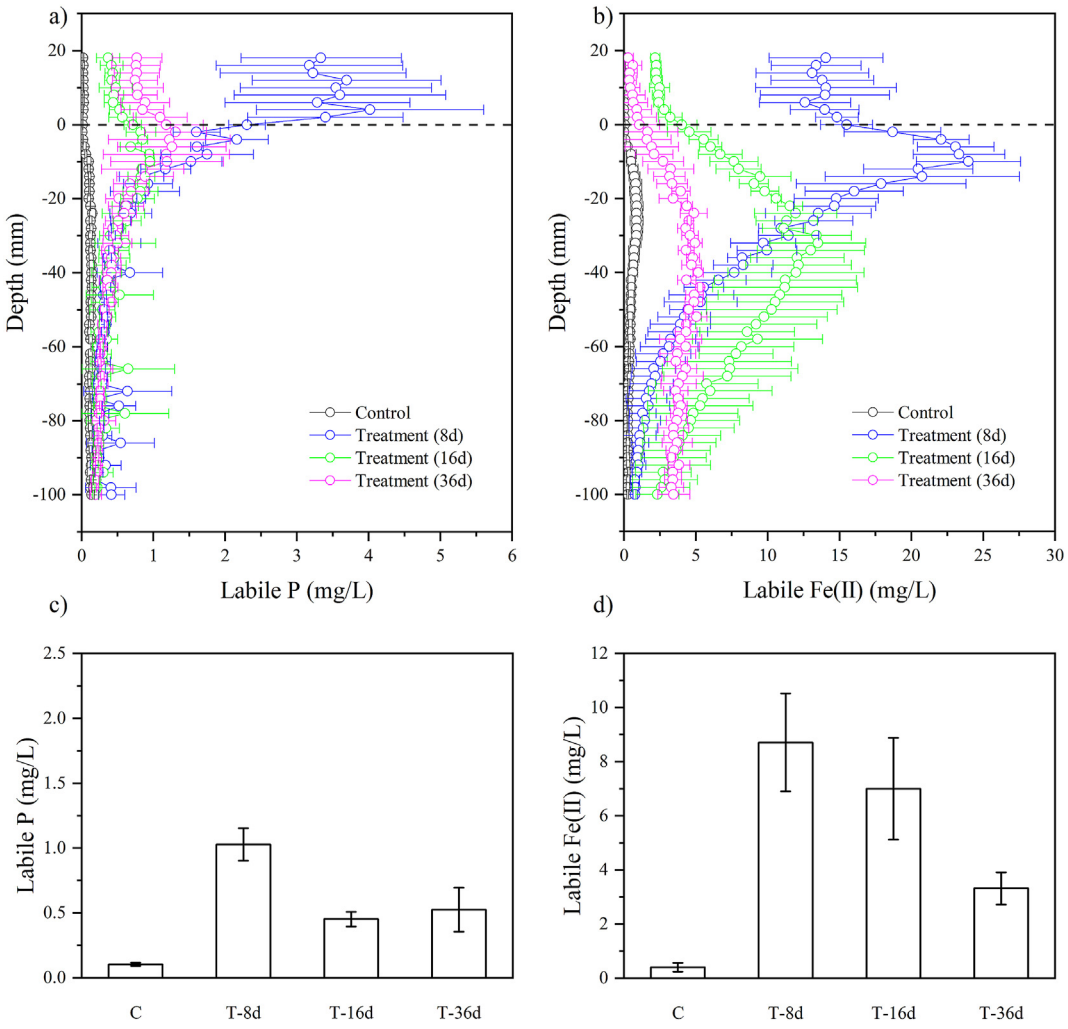

Fig. 4. Distribution of labile P (a) and labile Fe (b) in the sediment profiles and mean concentrations of labile P (c) and labile Fe (d) at the influence depth.

Table 3
Correlation analyses between labile P and labile Fe in sediments from the control and treatment groups.

Parameters	Treatments	Time	R^2	*P* value
Labile P vs. Labile Fe	Control		0.603**	<.01
	B. aeruginosa	8 days	0.596**	<.01
		16 days	0.227	0.081
		36 days	−0.654**	<.01

The average concentration of TP in the meat of one *B. aeruginosa* was 1420 mg/kg. During decomposition period, the conversion of organic P from *B. aeruginosa* to inorganic P contributed to the increase of SRP. However, this effect was short-lived at about 5 days (Fig. S1). The P content in benthic animals is limited relative to that in upper layer of sediments (Granéli and Solander, 1988). On the 8th day, P release from sediments was the main source of SRP (Fig. S1). The amount of SRP releasing from sediments on the 8th day was 630 mg/m^2. The interaction between Fe, P and S(−II) under anaerobic conditions is generally considered to be an important factor controlling the sediments P cycle (Meng et al., 2019). During *B. aeruginosa* decomposition stage, the DO concentration in the whole system was maintained in a low level, and P and Fe(II) significantly increased (Figs. 2–4). The largest increase in labile P concentrations was observed near the SWI in the sediment profiles

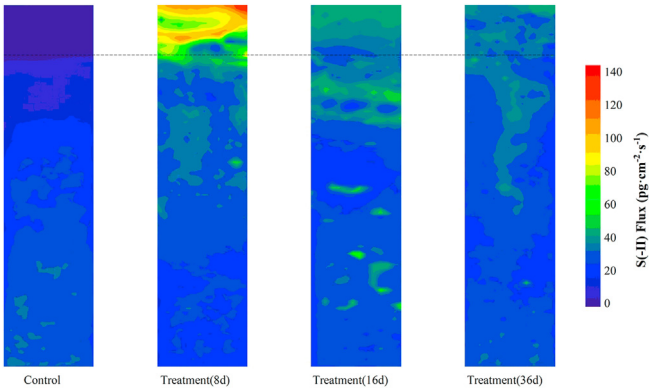

Fig. 5. Two-dimensional distribution of labile S(−II) in the sediments of the control and the treatment groups of days 8, 16, and 36.

(Fig. 4), suggesting that P was desorbed from Fe(III) oxides under the anaerobic conditions. It was also supported by the decrease of Fe−P in sediments on days 8 (Fig. S2). Meanwhile, reduction of sulfate to S(−II) caused an increase in labile S(−II) concentration (Table S1 and Fig. 5), the capture of Fe(II) by S(−II) can further aggravate the P release. The Fe-reduced P release and the indirect

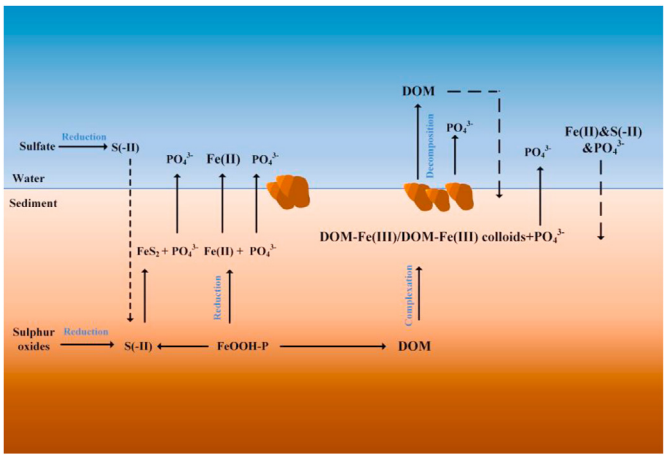

Fig. 6. Cycling of P, Fe, S, and DOM at the SWI during *B. aeruginosa* decomposition. DOM-Fe(III) presents formations of DOM with Fe(III).

effect of sulfur on P release were confirmed by the positive correlation between Fe and P (Tables 1–3) and consistent changes between labile S(−II) and labile Fe(II) (Figs. 4 and 5), respectively. These two reduction processes were frequently reported, based on previous study, the reduction condition resulted in the dissolution of Fe(III) oxides and the formation of FeS (or FeS_2), thereby increasing the P concentration in the waterbody (Han et al., 2020; Pan et al., 2019; Yuan et al., 2020).

Previous study found that the increase of DOM was accompanied by the decrease of iron minerals (Chen et al., 2006). DOM can reduction or leach out Fe(III) ion from iron minerals and combine to form soluble complexes (Sharma et al., 2010). Moreover, DOM can disperse iron mineral aggregates by wrapping or complexing iron mineral particles to form colloids (Tadanier et al., 2005; Yan et al., 2016). This was supported by the significant increase in DOM and dissolved Fe(II) during the decomposition of *B. aeruginosa* (Fig. 3). The interaction between DOM and iron minerals play an important role on the activation of As adsorbed on the Fe(III) oxyhydroxides in aquatic systems (Mikutta and Kretzschmar, 2011), especially under the anaerobic conditions. Owing to the similar chemical properties of P and As (Liu et al., 2011; Rosen et al., 2011), the mobilization of P in sediments under the anaerobic conditions may be significantly affected by the increase of DOM during decomposition of *B. aeruginosa*. This was supported by the significant positive correlation between SRP and UV_{254} (Table 2).

Decomposition only had a short-term effect on the P concentration of the water body. With the slow reoxygenation of the water body, the P was gradually reduced by the adsorption of metal oxides which was supported by the decrease of SRP/labile P and dissolved Fe(II)/labile Fe(II) (Figs. 2–4) and the increase of Fe–P in sediments from 8th to 36th day (Fig. S2).

4. Conclusions

The decomposition of *B. aeruginosa* changed the chemical conditions near the SWI. During decomposition, the P, Fe, S(−II), and DOM levels greatly increased. Phosphorus mobility was derived by iron redox reactions. Decomposition of *B. aeruginosa* resulted in anaerobic and reducing conditions, and the reduction of Fe(III) and sulfate contributed to the high concentration of P in pore water. The high concentration of DOM may control the mobilization of P through complexation. This was supported by the simultaneous increasing in DOM and SRP and the significant positive relationship between them during the decomposition of *B. aeruginosa*. These nutrients and their interaction, enhanced by decomposition processes, largely influenced P cycling.

Author contribution

Musong Chen: Conceptualization, Methodology, Writing-Reviewing and Editing. Yuexia Wu: Conceptualization, Methodology. Xiaolei Xing: Data curation, Writing – original draft. Yazhou Tang: Investigation. Cai Li: Software, Validation.

Declaration of competing interest

The authors declare that they have no known competing financial interests or personal relationships that could have appeared to influence the work reported in this paper.

Acknowledgements

This study was supported by the National Key Research and Development Program of China (grant numbers 2019YFD0901100) and Natural Science Foundation of China and Jiangsu Province (grant numbers 41701568, BK20171518).

Appendix A. Supplementary data

Supplementary data to this article can be found online at https://doi.org/10.1016/j.envpol.2021.117104.

References

Barber, A., Lalonde, K., Mucci, A., Gelinas, Y., 2014. The role of iron in the diagenesis of organic carbon and nitrogen in sediments: a long-term incubation experiment. Mar. Chem. 162, 1–9.
Berezina, N.A., Maximov, A.A., Vladimirova, O.M., 2019. Influence of benthic invertebrates on phosphorus flux at the sediment-water interface in the easternmost Baltic Sea. Mar. Ecol. Prog. Ser. 608, 33–43.
Chelsky, A., Pitt, K.A., Ferguson, A.J.P., Bennett, W.W., Teasdale, P.R., Welsh, D.T., 2016. Decomposition of jellyfish carrion in situ: short-term impacts on infauna, benthic nutrient fluxes and sediment redox conditions. Sci. Total Environ. 566, 929–937.
Chen, M., Ding, S., Chen, X., Sun, Q., Fan, X., Lin, J., Ren, M., Yang, L., Zhang, C., 2018. Mechanisms driving phosphorus release during algal blooms based on hourly changes in iron and phosphorus concentrations in sediments. Water Res. 133, 153–164.
Chen, M.S., Ding, S.M., Liu, L., Xu, D., Gong, M.D., Tang, H., Zhang, C.S., 2016. Kinetics of phosphorus release from sediments and its relationship with iron speciation influenced by the mussel (Corbicula fluminea) bioturbation. Sci. Total Environ. 542, 833–840.
Chen, M.S., Ding, S.M., Liu, L., Xu, D., Han, C., Zhang, C.S., 2015. Iron-coupled inactivation of phosphorus in sediments by macrozoobenthos (chironomid larvae) bioturbation: evidences from high-resolution dynamic measurements. Environ. Pollut. 204, 241–247.
Chen, Z., Cai, Y., Solo-Gabriele, H., Snyder, G.H., Cisar, J.L., 2006. Interactions of arsenic and the dissolved substances derived from turf soils. Environ. Sci. Technol. 40, 4659–4665.
Ding, S., Wang, Y., Xu, D., Zhu, C., Zhang, C., 2013. Gel-based coloration technique for the submillimeter-scale imaging of labile phosphorus in sediments and soils with diffusive gradients in thin films. Environ. Sci. Technol. 47, 7821–7829.
Ding, S.M., Xu, D., Sun, Q., Yin, H.B., Zhang, C.S., 2010. Measurement of dissolved reactive phosphorus using the diffusive gradients in thin films technique with a high-capacity binding phase. Environ. Sci. Technol. 44, 8169–8174.
Du, Y.X., Zhang, Q.Y., Liu, Z.W., He, H., Lurling, M., Chen, M.S., Zhang, Y.L., 2019. Composition of dissolved organic matter controls interactions with La and Al ions: implications for phosphorus immobilization in eutrophic lakes. Environ. Pollut. 248, 36–47.
Feng, M.H., Ngwenya, B.T., Wang, L., Li, W., Olive, V., Ellam, R.M., 2011. Bacterial dissolution of fluorapatite as a possible source of elevated dissolved phosphate in the environment. Geochem. Cosmochim. Acta 75 (19), 5785–5796.
Gao, L., Zhang, L., Hou, J., Wei, Q., Fu, F., Shao, H., 2013. Decomposition of macroalgal blooms influences phosphorus release from the sediments and implications for coastal restoration in Swan Lake, Shandong, China. Ecol. Eng. 60, 19–28.
Gao, Y., Leermakers, M., Elskens, M., Billon, G., Ouddane, B., Fischer, J.C., Baeyens, W., 2007. High resolution profiles of thallium, manganese and iron assessed by DET and DGT techniques in riverine sediment pore waters. Sci. Total Environ. 373, 526–533.

Gautreau, E., Volatier, L., Nogaro, G., Gouze, E., Mermillod-Blondin, F., 2020. The influence of bioturbation and water column oxygenation on nutrient recycling in reservoir sediments. Hydrobiologia 847, 1027–1040.
Goyne, K.W., Jun, H.J., Anderson, S.H., Motavalli, P.R., 2008. Phosphorus and nitrogen sorption to soils in the presence of poultry litter-derived dissolved organic matter. J. Environ. Qual. 37, 154–163.
Granéli, W., Solander, D., 1988. Influence of aquatic macrophytes on phosphorus cycling in lakes. Hydrobiologia 170, 245–266.
Gu, P., Li, Q., Zhang, H., Luo, Xin, Zhang, W., Zheng, Z., Luo, Xingzhang, 2020. Effects of cyanobacteria on phosphorus cycling and other aquatic organisms in simulated eutrophic ecosystems. Water (Switzerland) 12, 2265.
Han, C.N., Qin, Y.W., Zheng, B.H., Ma, Y.Q., Yang, C.C., Liu, Z.C., Zhuang, D.K., Zhao, Y.M., 2020. Geochemistry of phosphorus release along transect of sediments from a tributary backwater zone in the Three Gorges Reservoir. Sci. Total Environ. 722, 136964.
Herschy, B., Chang, S.J., Blake, R., Lepland, A., Abbott-Lyon, H., Sampson, J., Atlas, Z., Kee, T.P., Pasek, M.A., 2018. Archean phosphorus liberation induced by iron redox geochemistry. Nat. Commun. 9, 1346.
Hunt, J.F., Ohno, T., He, Z.Q., Honeycutt, C.W., Dail, D.B., 2007. Inhibition of phosphorus sorption to goethite, gibbsite, and kaolin by fresh and decomposed organic matter. Biol. Fertil. Soils 44, 277–288.
Kraal, P., Burton, E.D., Rose, A.L., Kocar, B.D., Lockhart, R.S., Grice, K., Bush, R.T., Tan, E., Webb, S.M., 2015. Sedimentary iron-phosphorus cycling under contrasting redox conditions in a eutrophic estuary. Chem. Geol. 392, 19–31.
Krom, M.D., Sholkovitz, E.R., 1977. Nature and reactions of dissolved organic matter in the interstitial waters of marine sediments. Geochem. Cosmochim. Acta 41, 1565–1573.
Lance, E., Paty, C., Bormans, M., Brient, L., Gérard, C., 2007. Interactions between cyanobacteria and gastropods. II. Impact of toxic Planktothrix agardhii on the life-history traits of Lymnaea stagnalis. Aquat. Toxicol. 81, 389–396.
Li, C., Ding, S., Yang, L., Zhu, Q., Chen, M., Tsang, D.C.W., Cai, G., Feng, C., Wang, Y., Zhang, C., 2019. Planar optode: a two-dimensional imaging technique for studying spatial-temporal dynamics of solutes in sediment and soil. Earth Sci. Rev. 197, 102916.
Li, X., Song, J., Ma, Q., Li, N., Yuan, H., Duan, L., Qu, B., 2015. Experiments and evidences: jellyfish (Nemopilema nomurai) decomposing and nutrients (nitrogen and phosphorus) released. Acta Oceanol. Sin. 34, 1–12.
Liu, G.L., Fernandez, A., Cai, Y., 2011. Complexation of arsenite with humic acid in the presence of ferric iron. Environ. Sci. Technol. 45, 3210–3216.
Maar, M., Timmermann, K., Petersen, J.K., Gustafsson, K.E., Storm, L.M., 2010. A model study of the regulation of blue mussels by nutrient loadings and water column stability in a shallow estuary, the Limfjorden. J. Sea Res. 64, 322–333.
Meng, T., Zhu, M.X., Ma, W.W., Gan, Z.X., 2019. Sulfur, iron, and phosphorus geochemistry in an intertidal mudflat impacted by shellfish aquaculture. Environ. Sci. Pollut. Res. 26, 6460–6471.
Mikutta, C., Kretzschmar, R., 2011. Spectroscopic evidence for ternary complex formation between arsenate and ferric iron complexes of humic substances. Environ. Sci. Technol. 45, 9550–9557.
Nędzarek, A., Tórz, A., Rakusa-Suszczewski, S., Bonisławska, M., 2015. Nitrogen and phosphorus release during fish decomposition and implications for the ecosystem of maritime Antarctica. Polar Biol. 38, 733–740.
Paerl, H.W., Xu, H., McCarthy, M.J., Zhu, G.W., Qin, B.Q., Li, Y.P., Gardner, W.S., 2011. Controlling harmful cyanobacterial blooms in a hyper-eutrophic lake (Lake Taihu, China): the need for a dual nutrient (N & P) management strategy. Water Res. 45, 1973–1983.
Pan, F., Guo, Z.R., Cai, Y., Liu, H.T., Wu, J.Y., Fu, Y.Y., Wang, B., Gao, A.G., 2019. Kinetic exchange of remobilized phosphorus related to phosphorus-iron-sulfur biogeochemical coupling in coastal sediment. Water Resour. Res. 55, 10494–10517.
Qin, B., Paerl, H.W., Brookes, J.D., Liu, J., Jeppesen, E., Zhu, G., Zhang, Y., Xu, H., Shi, K., Deng, J., 2019. Why Lake Taihu continues to be plagued with cyanobacterial blooms through 10 years (2007–2017) efforts. Sci. Bull. 64, 354–356.
Rosen, B.P., Ajees, A.A., McDermott, T.R., 2011. Life and death with arsenic Arsenic life: an analysis of the recent report "A bacterium that can grow by using arsenic instead of phosphorus. Bioessays 33, 350–357.
Rydin, E., Welch, E.B., 1998. Aluminum dose required to inactivate phosphate in lake sediments. Water Res. 32 (10), 2969–2976.
Sannigrahi, P., Ingall, E.D., Benner, R., 2006. Nature and dynamics of phosphorus-containing components of marine dissolved and particulate organic matter. Geochem. Cosmochim. Acta 70, 5868–5882.
Sharma, P., Ofner, R., Kappler, A., 2010. Formation of binary and ternary colloids and dissolved complexes of organic matter, Fe and as. Environ. Sci. Technol. 44 (12), 4479–4485.
Stachowitsch, M., Riedel, B., Zuschin, M., Machan, R., 2007. Oxygen depletion and benthic mortalities: the first in situ experimental approach to documenting an elusive phenomenon. Limnol Oceanogr. Methods 5, 344–352.
Tabatabai, M., 1974. A rapid method for determination of sulfate in water samples. Environ. Lett. 7 (3), 237–243.
Tadanier, C.J., Schreiber, M.E., Roller, J.W., 2005. Arsenic mobilization through microbially mediated deflocculation of ferrihydrite. Environ. Sci. Technol. 39 (9), 3061–3068.
Tamura, H., Goto, K., Yotsuyanagi, T., Nagayama, M., 1974. Spectrophotometric determination of iron(II) with 1,10-phenanthroline in the presence of large amounts of iron(III). Talanta 21, 314–318.
Tang, C.Y., Li, Y.P., He, C., Acharya, K., 2020. Dynamic behavior of sediment resuspension and nutrients release in the shallow and wind-exposed Meiliang Bay of Lake Taihu. Sci. Total Environ. 708, 135131.
Tiehm, A., Hollert, H., Yin, D.Q., Zheng, B.H., 2019. Tai Hu (China): water quality and processes - from the source to the tap. Sci. Total Environ. 712, 135559.
Wang, J.Z., Jiang, X., Zheng, B.H., Chen, C.X., Kang, X.M., Zhang, C.Y., Song, Z.Q., Wang, K., Wang, W.W., Wang, S.H., 2016. Effect of algal bloom on phosphorus exchange at the sediment-water interface in Meiliang Bay of Taihu Lake, China. Environ. Earth Sci. 75 (57), 1–9.
Wang, J.Z., Jiang, X., Zheng, B.H., Niu, Y., Wang, K., Wang, W.W., Kardol, P., 2015. Effects of electron acceptors on soluble reactive phosphorus in the overlying water during algal decomposition. Environ. Sci. Pollut. Res. 22, 19507–19517.
Wang, S.R., Jiao, L.X., Yang, S.W., Jin, X.C., Yi, W.L., 2012. Effects of organic matter and submerged macrophytes on variations of alkaline phosphatase activity and phosphorus fractions in lake sediment. J. Environ. Manag. 113, 355–360.
Wang, Z.C., Huang, S., Li, D.H., 2019. Decomposition of cyanobacterial bloom contributes to the formation and distribution of iron-bound phosphorus (Fe-P): insight for cycling mechanism of internal phosphorus loading. Sci. Total Environ. 652, 696–708.
Wu, S.Q., He, S.B., Huang, J.C., Gu, J.Y., Zhou, W.L., Gao, L., 2017. Decomposition of emergent aquatic plant (cattail) litter under different conditions and the influence on water quality. Water Air Soil Pollut. 228 (2), 70.
Xie, C.S., Xu, J., Tang, J., Baig, S.A., Xu, X.H., 2013. Comparison of phosphorus determination methods by ion chromatography and molybdenum blue methods. Commun. Soil Sci. Plant Anal. 44, 2535–2545.
Xu, D., Wu, W., Ding, S.M., Sun, Q., Zhang, C.S., 2012. A high-resolution dialysis technique for rapid determination of dissolved reactive phosphate and ferrous iron in pore water of sediments. Sci. Total Environ. 421, 245–252.
Xu, H., Guo, L., 2017. Molecular size-dependent abundance and composition of dissolved organic matter in river, lake and sea waters. Water Res. 117, 115–126.
Yan, J.L., Jiang, T., Yao, Y., Lu, S., Wang, Q.L., Wei, S.Q., 2016. Preliminary investigation of phosphorus adsorption onto two types of iron oxide-organic matter complexes. J. Environ. Sci. 42, 152–162.
Yao, Y., Wang, P., Wang, C., Hou, J., Miao, L., Yuan, Y., Wang, T., Liu, C., 2016. Assessment of mobilization of labile phosphorus and iron across sediment-water interface in a shallow lake (Hongze) based on in situ high-resolution measurement. Environ. Pollut. 219, 873–882.
Yuan, H.Z., An, S.Q., Shen, J., Liu, E.F., 2014. The characteristic and environmental pollution records of phosphorus species in different trophic regions of Taihu Lake, China. Environ. Earth Sci. 71, 783–792.
Yuan, H.Z., Tai, Z.Q., Li, Q., Liu, E.F., 2020. In-situ, high-resolution evidence from water-sediment interface for significant role of iron bound phosphorus in eutrophic lake. Sci. Total Environ. 706, 136040.
Zhang, S., Fang, X., Zhang, J.B., Yin, F., Zhang, H., Wu, L.Z., Kitazawa, D., 2020a. The effect of bioturbation activity of the ark clam scapharca subcrenata on the fluxes of nutrient exchange at the sediment-water interface. J. Ocean Univ. China 19, 232–240.
Zhang, W.Q., Jin, X., Meng, X., Tang, W.Z., Shan, B.Q., 2018a. Phosphorus transformations at the sediment-water interface in shallow freshwater ecosystems caused by decomposition of plant debris. Chemosphere 201, 328–334.
Zhang, W.Q., Zhu, X.L., Jin, X., Meng, X., Tang, W.Z., Shan, B.Q., 2017. Evidence for organic phosphorus activation and transformation at the sediment-water interface during plant debris decomposition. Sci. Total Environ. 583, 458–465.
Zhang, W.Z., Gu, P., Zhu, W.J., Jing, C.S., He, J., Yang, X.Y., Zhou, L., Zheng, Z., 2020b. Effects of cyanobacterial accumulation and decomposition on the microenvironment in water and sediment. J. Soils Sediments 20, 2510–2525.
Zhang, Y., Zhou, Y., Shi, K., Qin, B., Yao, X., Zhang, Y., 2018b. Optical properties and composition changes in chromophoric dissolved organic matter along trophic gradients: implications for monitoring and assessing lake eutrophication. Water Res. 131, 255–263.